Supporting Information

Bis-(*N*-aminoethylethanolamine)-Copper (II) nano catalysis (AEEA-Cu(II)-Nps) meditated to synthesis a series of 2-thioxo-1,2,3,4-tetrahydropyrimidine-5-carboxamide derivatives: characterization of theoretical, Computational and evaluation of molecular docking, and cytotoxicity activities

2. Materiel and methods

2.1. Chemistry

General materials and characterization techniques:

Material was supplied by Nice and Loba chemicals. An open capillary tube was used to measure the melting point of the material. Shimadzu 8201PC (4000-400 cm^{-1}) of IR spectrometer was recorded. The ^{1}H NMR and ^{13}C NMR spectra were measured using a JEOL-300 MHz NMR spectrometer. With an Elementer machine (Varian EL III), we recorded the elemental analyses (C, H, and N). The purity of compounds was determined using Thin-layer chromatography (TLC) was performed on silica gel plates, and to determine the purity of the compounds

2.Synthesis of 6-methyl-4-phenyl-2-thioxo-1,2,3,4-tetrahydro-pyrimidine-5-carboxylic acid hydrazide (1a)

Yellow solid; Yield: 98 % (0.94g); mw: 262.33; mp: 264°C; IR (cm^{-1}): 3358(NH), 3179(Ar-H), 2724 (Ph-CHstr), 1100 (C=S), 1625 (CONH); ^{1}H NMR (300MHz): δ 9.40 (s, 1H, CSNH), 9.20 (s, 2H, NH), 7.20 (t, 2H, *J*=6.23Hz, Ph), 6.20 (d, 2H, *J*=6.21Hz, Ph), 5.48 (t, 1H, *J*=6.23Hz, Ph), 4.20 (1H, s, C-4), 2.1 (2H, s, NH_2), 1.20 (s, 3H, CH_3); ^{13}C NMR (300MHz): 174.2 (-<u>C</u>=S), 165.0 (- <u>C</u>=O), 158.0 (-<u>C</u>H), 142.0, 127.1, 128.3, 126.5 (6C, Ar ring), 100.0 (1C, 5C-H), 54.0 (1C, 4C-H), 14.0 (1C, -CH_3); EI-MS (m/z): 263.09 (M^{+},15%); Elemental analysis: Calcd. For ($C_{12}H_{14}N_4OS$): C, 54.94; H, 5.38; N, 21.36%; Found: C, 54.90; H, 5.32; N, 21.34%.

***N*'-benzylidene-6-methyl-4-phenyl-2-thioxo-1,2,3,4-tetrahydropyrimidine-5-carbo hydrazide (1b)**

Brown solid; Yield: 94 % (0.90g); mw: 350.44; mp: 286°C; IR (cm^{-1}): 3356 (NH), 3172 (Ar-H), 2726 (Ph-CHstr), 1104 (C=S), 1627 (CONH); ^{1}H NMR (300MHz): δ 9.42 (s, 1H, CSNH), 8.54 (s, 1H, -CH=N), 8.20 (s, 2H, NH), 7.83 (t, 2H, *J*=6.23Hz, Ph), 7.50 (m, 3H, Ph), 7.33 (t, 2H, *J*=6.23Hz, Ar), 7.24 (t, 1H, *J*=6.23Hz, Ar), 7.23 (d, 2H, *J*=6.21Hz, Ar), 5.40 (s, 1H, CH-Ph),

2.26 (s, 3H, CH_3); ^{13}C NMR (300MHz): 174.1 (-C=S), 168.0, 159.1, 146.8 (-C=N), 143.1, 128.3, 126.8, 126.3 (phenyl ring), 133.1, 132.0, 128.7, 128.1 (6C, Ph ring), 106.2 (-C-CO), 59.2 (-C-Ph), 18.6 (-CH_3); EI-MS (m/z): 351.12 (M^+,23%); Elemental analysis: Calcd. For ($C_{19}H_{18}N_4OS$): C, 65.12; H, 5.18; N, 15.99%; Found: C, 65.10; H, 5.20; N, 15.96%.

6-Methyl-4-phenyl-N'-(3-phenylallylidene)-2-thioxo-1,2,3,4-tetrahydropyrimidine-5-carbohydrazide (1c)

Yellow solid; Yield: 92 % (0.86g); mw: 376.47; mp: 272°C; IR (cm^{-1}): 3358 (NH), 3176 (Ar-H), 2724 (Ph-CHstr), 1106 (C=S), 1628 (CONH); ^1H NMR (300MHz): δ 9.40 (s, 1H, CSNH), 8.24 (s, 2H, NH), 7.60 (2H, d, *J*=6.21Hz, Ph), 7.50 (1H, s, -CH=N), 7.40 (t, 2H, *J*=6.23Hz, Ph), 7.33 (t, 1H, *J*=6.23Hz, Ph), 7.33 (t, 2H, *J*=6.23Hz, Ar), 7.26 (t, 1H, *J*=6.23Hz, Ar), 7.23 (d, 2H, *J*=6.21Hz, Ar), 7.22 (s, 1H, =CH), 6.85 (s, 1H, =CH), 5.40 (s, 1H, CH-Ph), 2.26 (s, 3H, CH_3); ^{13}C NMR (300MHz): 174.1, 168.2, 159.3, 137.2, 143.1, 127.4, 126.5, 125.2 (6C, Ar ring), 135.1, 128.3, 127.4, 126.2 (6C, Ph ring), 134.1, 126.3 , 106.4 (-C-CO), 59.2 (-C-Ph), 18.8 (1C, -CH_3); EI-MS (m/z): 377.14 (M^+,24%); Elemental analysis: ($C_{21}H_{20}N_4OS$): Calcd. C, 67.00; H, 5.35; N, 14.88%; Found: C, 67.04; H, 5.33; N, 14.90%.

6-Methyl-N',4-diphenyl-2-thioxo-1,2,3,4-tetrahydropyrimidine-5-carbohydrazide (1d)

Yellow solid; Yield: 86 % (0.82g); mw: 338.43; mp: 186°C; IR (cm^{-1}): 3356 (NH), 3174 (Ar-H), 2720 (Ph-CHstr), 1108 (C=S), 1624 (CONH); ^1H NMR (300MHz): δ 9.42 (s, 1H, CSNH), 8.26 (s, 3H, NH), 7.36 (t, 2H, *J*=6.23Hz, Ph), 7.06 (d, 2H, *J*=6.21Hz, Ph), 6.90 (t, 1H, *J*=6.23Hz, Ph), 7.33 (t, 2H, *J*=6.23Hz, Ar), 7.26 (t, 1H, *J*=6.23Hz, Ar), 7.23 (d, 2H, *J*=6.21Hz, Ar), 5.42 (s, 1H, CH-Ph), 2.26 (s, 3H, CH_3); ^{13}C NMR (300MHz): 174.1, 165.2, 159.1, 142.8, 127.2, 126.5, 126.3 (Phenyl ring), 149.0, 128.9, 122.6, 113.1 (Phenyl ring), 106.2 (1C, C-CO), 59.0 (-C-Ph), 18.4; EI-MS (m/z): 339.12 (M^+,22%); Elemental analysis: ($C_{18}H_{18}N_4OS$): Calcd. C, 63.88; H, 5.36; N, 16.56%; Found: C, 63.86; H, 5.33; N, 16.58%.

6-Methyl-N,4-diphenyl-2-thioxo-1,2,3,4-tetrahydropyrimidine-5-carboxamide (1e)

Dust white solid; Yield: 90 % (0.88g); mw: 323.41; mp: 186°C; IR (cm^{-1}): 3358 (NH), 3172 (Ar-H), 2724 (Ph-CHstr), 1110 (C=S), 1626 (CONH); ^1H NMR (300MHz): δ 9.46 (1H, s, CSNH), 8.24 (s, 2H, NH), 7.61 (t, 2H, *J*=6.23Hz, Ph), 7.43 (d, 2H, *J*=6.21Hz, Ph), 7.19 (t, 1H,

J=6.23Hz, Ph), 7.33 (t, 2H, *J*=6.23Hz, Ar), 7.26 (t, 1H, *J*=6.23Hz, Ar), 7.23 (d, 2H, *J*=6.21Hz, Ar), 5.40 (s, 1H, CH-Ph), 2.24 (s, 3H, CH_3); ^{13}C NMR (300MHz): 174.3, 163.1, 159.4, 143.7, 127.9, 127.1, 126.1 (Phenyl ring), 137.6, 128.9, 128.0, 121.6 (6C, Ph ring), 106.4 (-C-CO), 58.9 (-C-Ph), 17.9 (-CH_3); EI-MS (m/z): 324.11 (M^+,21%); Elemental analysis: ($C_{18}H_{17}N_3OS$): Calcd. C, 66.85; H, 5.30; N, 12.99%; Found: C, 66.83; H, 5.33; N, 12.96%.

N-(benzylidenecarbamothioyl)-6-methyl-4-phenyl-2-thioxo-1,2,3,4-tetrahydro pyrimidine-5-carboxamide (1f)

Brown solid; Yield: 82 % (0.78g); mw: 394.51; mp: 226°C; IR (cm^{-1}): 3356 (NH), 3172 (Ar-H), 2726 (Ph-CHstr), 1104 (C=S), 1627 (CONH); ^{1}H NMR (300MHz): δ 9.42 (s, 1H, CSNH), 9.46 (s, 1H, -CH=N), 8.20 (s, -NH), 7.83 (t, 2H, *J*=6.23Hz, Ph), 7.54(m, 3H, Ph), 7.33 (t, 2H, *J*=6.23Hz, Ar), 7.27(t, 1H, *J*=6.23Hz, Ar), 7.23 (d, 2H, *J*=6.21Hz, Ar), 5.46 (s, 1H, CH-Ph), 2.26 (3H, s,CH_3); ^{13}C NMR (300MHz): 191.3 (1C, C=S), 174.1, 173.5, 159.1, 163.7 (-C=N), 142.9, 127.2, 126.3, 126.0 (Phenyl ring), 133.2, 132.2, 129.1, 126.9 (Phenyl ring), 106.4 (-C-CO), 59.2 (-C-Ph), 17.9 (-CH_3); EI-MS (m/z): 395.10 (M^+,22%); Elemental analysis: ($C_{20}H_{18}N_4OS_2$): Calcd. C, 60.89; H, 4.60; N, 14.20%; Found: C, 60.86; H, 4.62; N, 14.24%.

6-Methyl-4-phenyl-N-(5-phenylpenta-2,4-dienethioyl)-2-thioxo-1,2,3,4-tetrahydro pyrimidine-5-carboxamide (1g)

Yellow solid; Yield: 96 % (0.92g); mw: 420.55; mp: 292°C; IR (cm^{-1}): 3358 (NH), 3176 (Ar-H), 2724 (Ph-CHstr), 1106 (C=S), 1628 (CONH); ^{1}H NMR (300MHz): δ 9.40 (s, 1H, CSNH), 8.24 (s, 2H, NH), 7.60 (d, 2H, *J*=6.21Hz, Ph), 7.50 (s, 1H,-CH=N), 7.40 (t, 2H, *J*=6.23Hz, Ph), 7.33 (t, 1H, *J*=6.23Hz, Ph), 7.33 (t, 2H, *J*=6.23Hz, Ar), 7.26 (t, 1H, *J*=6.23Hz, Ar), 7.23 (d, 2H, *J*=6.21Hz, Ar), 7.03 (s, 1H, =CH), 5.24 (s, 1H, =CH), 5.40 (s, 1H, CH-Ph), 2.24 (s, 3H, CH_3); ^{13}C NMR (300MHz): 191.3 (-C=S), 174.1, 173.5, 159.1, 164.1 (-C=N), 143.7, 128.4, 126.6, 126.1 (Phenyl ring), 135.6, 127.5, 128.1, 127.1 (Phenyl ring), 133.1 (-C=C), 119.5 (-C=C), 106.1 (-C-CO), 59.0 (-C-Ph), 17.9; EI-MS (m/z): 421.11 (M^+,26%); Elemental analysis: ($C_{22}H_{20}N_4OS_2$): Calcd. C, 62.83; H, 4.79; N, 13.32%; Found: C, 62.80; H, 4.80; N, 13.32%.

6-Methyl-N-(naphthalen-2-yl)-4-phenyl-2-thioxo-1,2,3,4-tetrahydropyrimidine-5-carboxamide (1h)

Black solid; Yield: 90 % (0.94g); mw: 373.47; mp: 182°C; IR (cm^{-1}): 3356 (NH), 3172 (Ar-H), 2726 (Ph-CHstr), 1104 (C=S), 1627 (CONH); ^{1}H NMR (300MHz): δ 9.42 (1H, s, CSNH), 8.20 (2H, s, NH), 8.29-7.36 (7H, m, Naphthyl ring), 7.33 (t, 2H, *J*=6.23Hz), 7.26 (t, 1H, *J*=6.23Hz), 7.23 (d, 2H, *J*=6.21Hz), 5.40 (s, 1H, CH-Ph), 2.24 (s, 3H, CH_3); ^{13}C NMR (300MHz): 174.1, 163.1, 159.1, 143.6, 128.1, 125.1 , 125.6 (Phenyl ring), 135.4, 132.1, 127.3, 126.2, 126.1, 125.0, 124.1, 121.3, 119.8, 116.7 (10C, Naphthyl ring), 106.4 (-C-CO), 58.9 (-C-Ph), 17.9 (-CH_3); EI-MS (m/z): 374.13 (M^+,24%); Elemental analysis:($C_{22}H_{19}N_3OS$): Calcd. C, 70.75; H, 5.13; N, 11.25%; Found: C, 70.73; H, 5.10; N, 11.27%.

6-Methyl-4-phenyl-2-thioxo-N-(p-tolyl)-1,2,3,4-tetrahydropyrimidine-5-carbox amide (1i)

Yellow solid; Yield: 80 % (0.74g); mw: 337.44; mp: 142°C; IR (cm^{-1}): 3358 (NH), 3172 (Ar-H), 2724 (Ph-CHstr), 1106 (C=S), 1620 (CONH); ^{1}H NMR (300MHz): δ 9.42 (s, 1H, CSNH), 8.26 (s, 2H, NH), 7.19 (d, 2H, *J*=6.21Hz, Ph), 7.17 (d, 2H, *J*=6.21Hz, Ph), 7.33 (t, 2H, *J*=6.23Hz, Ar), 7.26 (1H, t, *J*=6.23Hz, Ar), 7.23 (d, 2H, *J*=6.21Hz, Ar), 5.42 (s, 1H, CH-Ph), 2.34 (s, 3H, CH_3), 2.26(s, 3H, CH_3); ^{13}C NMR (300MHz): 174.1, 163.1, 159.1 (1C, -C=C), 142.9, 127.4, 125.1, 125.2 (6C, Ar ring), 136.8, 134.6, 129.2, 121.5 (6C, Ph ring), 106.2 (-C-CO), 58.9 (-C-Ph), 21.3, 17.9; EI-MS (m/z): 338.13 (M^+,21%); Elemental analysis: ($C_{19}H_{19}N_3OS$): Calcd. C, 67.63; H, 5.68; N, 12.45%; Found: C, 67.60; H, 5.70; N, 12.43%.

N-acetyl-6-methyl-4-phenyl-2-thioxo-1,2,3,4-tetrahydropyrimidine-5-carboxamide (1j)

Brown solid; Yield: 82 % (0.76g); mw: 289.35; mp: 154°C; IR (cm^{-1}): 3356 (NH), 3170 (Ar-H), 2722 (Ph-CHstr), 1104 (C=S), 1622 (CONH); ^{1}H NMR (300MHz): δ 9.40 (s, 1H, CSNH), 8.24 (s, 2H, NH), 7.31 (t, 2H, *J*=6.23Hz, Ar), 7.26 (t, 1H, *J*=6.23Hz, Ar), 7.23 (d, 2H, *J*=6.21Hz, Ar), 5.40 (s, 1H, CH-Ph), 2.26 (s, 3H, CH_3), 2.24 (s, 3H, CH_3); ^{13}C NMR (300MHz): 174.1 (-C=S), 171.5 (-C=O), 169.8 (-C=O), 159.1 (-C=C), 142.6, 127.9, 126.1, 126.3 (6C, Ar ring), 106.2 (1C, C-CO), 58.6 (-C-Ph), 22.8 (-CH_3), 17.9 (-CH_3); EI-MS (m/z): 290.09 (M^+,17%); Elemental analysis: ($C_{14}H_{15}N_3O_2S$): Calcd. C, 58.11; H, 5.23; N, 14.52%; Found: C, 58.13; H, 5.20; N, 14.50%.

N-carbamoyl-6-methyl-4-phenyl-2-thioxo-1,2,3,4-tetrahydropyrimidine-5-carbox amide (1k)

Brown solid; Yield: 86 % (0.80g); mw: 351.42; mp: 176°C; IR (cm^{-1}): 3360 (NH), 3174 (Ar-H), 2726 (Ph-CHstr), 1108 (C=S), 1626 (CONH); ^{1}H NMR (300MHz): δ 9.42 (1H, s, CSNH), 8.20 (2H, s, NH), 8.03 (d, 2H, *J*=6.21Hz, Ph), 7.70 (t, 1H, *J*=6.23Hz, Ph), 7.63 (t, 2H, *J*=6.23Hz, Ph), 7.33 (t, 2H, *J*=6.23Hz, Ar), 7.26 (t, 1H, *J*=6.23Hz, Ar), 7.23 (d, 2H, *J*=6.21Hz, Ar), 5.40 (s, 1H, CH-Ph), 2.28 (s, 3H, CH_3); ^{13}C NMR (300MHz): 174.1, 171.5, 170.6, 159.1, 143.3, 127.5, 126.5, 126.2 (-Phenyl ring), 133.6, 132.3, 128.5, 127.1 (6C, Ph), 106.2 (-C-CO), 58.6 (-CH-Ph), 17.9; EI-MS (m/z): 352.11 (M^{+},21%); Elemental analysis: ($C_{19}H_{17}N_3O_2S$): Calcd. C, 64.94; H, 4.88; N, 11.96%; Found: C, 64.96; H, 4.86; N, 11.94%.

N-carbamoyl-6-methyl-4-phenyl-2-thioxo-1,2,3,4-tetrahydropyrimidine-5-carboxamide (1l)

White solid; Yield: 83 % (0.77g); mw: 290.34; mp: 164°C; IR (cm^{-1}): 3360 (NH), 3174 (Ar-H), 2726 (Ph-CHstr), 1108 (C=S), 1626 (CONH); ^{1}H NMR (300MHz): δ 9.42 (s, 1H, CSNH), 8.20 (s, 2H, NH), 7.33 (t, 2H, *J*=6.23Hz, Ar), 7.22 (t, 1H, *J*=6.23Hz), 7.23 (d, 2H, *J*=6.21Hz, Ar), 6.04 (s, 2H, NH_2), 5.40 (s, 1H, CH-Ph), 2.26 (s, 3H, CH_3); ^{13}C NMR (300MHz): 174.1 (-C=S), 171.5, 152.9, 159.1, 142.9, 127.3, 126.2, 125.2 (6C, Ar ring), 106.2 (-C-CO), 58.2 (-C-Ph), 17.9; EI-MS (m/z): 291.09 (M^{+},14%); Elemental analysis: ($C_{13}H_{14}N_4O_2S$): Calcd. C, 53.78; H, 4.86; N, 19.30%; Found: C, 53.75; H, 4.84; N, 19.32%.

***N*-(benzylidenecarbamoyl)-6-methyl-4-phenyl-2-thioxo-1,2,3,4-tetrahydropyrimidine-5-carboxamide (1m)**

Yellow solid; Yield: 78 % (0.72g); mw: 378.45; mp: 216°C; IR (cm^{-1}): 3358 (NH), 3172 (Ar-H), 2724 (Ph-CHstr), 1106 (C=S), 1620 (CONH); ^{1}H NMR (300MHz): δ 9.48 (s, 1H, CH=N), 9.42 (s, 1H, CSNH), 8.26 (s, 2H, NH), 7.83 (d, 2H, *J*=6.21Hz, Ph), 7.54 (m, 3H, Ph), 7.33 (t, 2H, *J*=6.23Hz, Ar), 7.25 (t, 1H, *J*=6.23Hz, Ar), 7.23 (d, 2H, *J*=6.21Hz, Ar), 5.40 (s, 1H, CH-Ph), 2.25(s, 3H, CH_3); ^{13}C NMR (300MHz): 174.1, 171.5, 164.1, 163.7, 159.1 (-C=C), 144.1, 128.1, 127.2, 126.2 (-Phenyl ring), 133.1, 131.6, 128.1, 127.9 (6C, Ph ring), 106.4 (-C-CO), 58.2 (-C-Ph), 17.9; EI-MS (m/z): 379.12 (M^{+},22%); Elemental analysis: ($C_{20}H_{18}N_4O_2S$): Calcd. C, 63.47; H, 4.79; N, 14.80%; Found: C, 63.50; H, 4.76; N, 14.82%.

6-Methyl-4-phenyl-*N*-(3-phenylallylidene)carbamoyl)-2-thioxo-1,2,3,4-tetrahydro pyrimidine-5-carboxamide (1n)

Brown solid; Yield: 72 % (0.66g); mw: 404.48; mp: 294°C; IR (cm^{-1}): 3360 (NH), 3174 (Ar-H), 2726 (Ph-CHstr), 1108 (C=S), 1622 (CONH); ^{1}H NMR (300MHz): δ 9.42 (s, 1H, CSNH), 8.26 (s, 2H, NH), 7.60 (d, 2H, *J*=6.21Hz, Ph), 7.36(t, 2H, *J*=6.23Hz, Ph), 7.33 (t, 1H, *J*=6.23Hz, Ph), 7.50 (s, 1H, CH=N), 7.33 (t, 2H, *J*=6.23Hz, Ar), 7.26 (t, 1H, *J*=6.23Hz, Ar), 7.23 (d, 2H, *J*=6.21Hz, Ar), 7.03 (s, 1H, =CH), 5.40 (1H, s, CH-Ph), 5.24 (1H, s, =CH), 2.26 (3H, s,CH_3); ^{13}C NMR (300MHz): 174.1, 171.5, 164.1, 163.7, 159.1, 143.1, 128.7, 126.9, 125.2 (Phenyl ring), 135.6, 127.9, 127.1, 126.9 (6C, Ph ring), 133.3 (1C, -C=C), 119.9 (1C, -C=C), 106.4 (1C, C-CO), 58.2, 17.9; EI-MS (m/z): 405.13 (M^+,26%); Elemental analysis: ($C_{22}H_{20}N_4O_2S$) Calcd. C, 65.33; H, 4.98; N, 13.85%; Found: C, 65.30; H, 4.96; N, 13.87%.

***N*,6-dimethyl-4-phenyl-2-thioxo-1,2,3,4-tetrahydropyrimidine-5-carboxamide (1o)**

Dust white solid; Yield: 87 % (0.86g); mw: 261.34; mp: 208°C; IR (cm^{-1}): 3358 (NH), 3179 (Ar-H), 2724 (Ph-CHstr), 1100 (C=S), 1625 (CONH); ^{1}H NMR (300MHz): δ 9.40 (s, 1H, CSNH), 9.20 (s, 2H, NH), 7.33 (t, 2H, *J*=6.23Hz, Ph), 7.26 (t, 1H, *J*=6.23Hz, Ph), 7.23 (d, 2H, *J*=6.21Hz, Ph), 5.38 (s, 1H, CH-Ph), 2.73 (s, 3H, CH_3), 2.26 (s, 3H, CH_3); ^{13}C NMR (300MHz): 174.1 (-C=S), 168.5, 159.1, 143.6, 128.1, 126.7, 125.2 (6C, Ar ring), 106.4, 58. 8, 26.5 (-CH_3), 17.7; EI-MS (m/z): 262.10 (M^+,14%); Elemental analysis: ($C_{13}H_{15}N_3OS$): Calcd. C, 54.74; H, 5.79; N, 16.08%; Found: C, 54.76; H, 5.80; N, 16.10%.

2.1.3. GC-EI-MS Instrumentation

Single quadrupole GC-EI-MS perkin Elmer GCMS model GC clarus 680 and MS SQ8T (EI) with used Elite-5 (5% diphenyl/95% dimethyl polysiloxane) capillary columns - 30 m x 0.25 mm x 0.25µm. The GC-EI-MS data indicate a volume of injection 1 mL; a temperature of 250°C; and a split ratio of 20:1; and the split ratio was 20:1. Temperature was initially set at 800ºC (1 min hold), ramped to 280ºC at 15ºC/min, and held for 2 minutes. Carriers gas (helium) was injected at 1 mL/minute at 280°C when this experiment was performed. After a solvent delay of two minutes, scan rates of 1,500 Da/s were used for the mass spectrometer to scan from m/z 50 to 500. In this experiment, the source and the quadrupole were each at 250°C and 200°C, respectively.

2.1.4. Computational methods

An ab initio CBS-QB3 model (Montgomery et al., 1991) was used to elevate geometry and calculate frequency using the hybrid density functional theory (DFT) of Becke's three-parameter (B3) exchange-Lee, Yang, and Parr (LYP) correlation functional (B3LYP) (Becke, 1993; Lee et al., 1988; Stephens et al., 1994) in conjunction with the 6-311G(d,p) basis set (Hariharan and Pople, 1973) and CCSD(T) follows to get limit of basis sets. For this study, a highly accurate method along with relatively low computational costs has been selected in order to achieve high accuracy. The optimization of molecular geometry in gas phase was done in conjunction with vibrational analysis, and frontier orbital calculations (HOMO-LUMO) using B3LYP (Becke, 1993) and Gaussian 09 package (Frisch et al., 2010) was used to set the 6 - 311G(d,p) basis. The electronic spectrum was designed using time-dependent density functional theory (TD-DFT) and the hybrid exchange correlation function of B3LYP (Becke, 1993) over 6-311G (d,p) basis sets. By subtracting the TMS shielding constants, NMR chemical shifts of each conformer were obtained utilizing the GIAO (Gauge-Independent Atomic Orbital) (Rohlfing et al., 1984; Wolinski et al., 1990). Simulations conducted within the gas phase have been performed using the PCM (Polarized Continuum Model) (Foresman et al., 1996; Tomasi et al., 2005). MEP diagrams have been designed for assess the chemical reactivity and intramolecular interactions.

2.1.4. Computational methods

An ab initio CBS-QB3 model (Montgomery et al., 1991) was used to elevate geometry and calculate frequency using the hybrid density functional theory (DFT) of Becke's three-parameter (B3) exchange-Lee, Yang, and Parr (LYP) correlation functional (B3LYP) (Becke, 1993; Lee et al., 1988; Stephens et al., 1994) in conjunction with the 6-311G(d,p) basis set (Hariharan and Pople, 1973) and CCSD(T) follows to get limit of basis sets. Experimental details available in

For this study, a highly accurate method along with relatively low computational costs has been selected in order to achieve high accuracy. The optimization of molecular geometry in gas phase was done in conjunction with vibrational analysis, and frontier orbital calculations (HOMO-LUMO) using B3LYP (Becke, 1993) and Gaussian 09 package (Frisch et al., 2010) was used to set the 6 - 311G(d,p) basis. The electronic spectrum was designed using time-dependent density functional theory (TD-DFT) and the hybrid exchange correlation function of B3LYP (Becke, 1993) over 6-311G (d,p) basis sets. By subtracting the TMS shielding constants, NMR chemical

shifts of each conformer were obtained utilizing the GIAO (Gauge-Independent Atomic Orbital) (Rohlfing et al., 1984; Wolinski et al., 1990). Simulations conducted within the gas phase have been performed using the PCM (Polarized Continuum Model) (Foresman et al., 1996; Tomasi et al., 2005). MEP diagrams have been designed for assess the chemical reactivity and intramolecular interactions.

2.1.5. Cytotoxic activity

On the basis of previous literature, cytotoxic properties of the newly synthesized compounds (**1a-1o**) were analysed (Surendra Kumar et al., 2017). The newly synthesized compounds (1a-10) were screened for their cytotoxic activity according to a previously published procedure.. Compounds (100 µM) were incubated in a microtiter plate with three different cell lines for 72 h, and cell viability was assessed by MTT assay. The three cell lines were HepG2 (liver), MCF-7(breast), and HeLa(cervical). The percentage of growth of the treated cells compared to that of the untreated control cells was calculated. Compounds that reduced the growth of a cell line by 32% or morewere considered to have antitumor activity.

The measured 0.1mL of the cell suspension (containing 5×10^{6} cells/100µL) and 0.1mL of the test solution (6.25-100µg 1% DMSO such that the final concentration of DMSO in media was less than 1%) were added to the 27 well plates and kept in a 5% CO_2 incubator at 37°C for 72 hr. The blank contained only cell suspension and control wells contained 1% DMSO and cell suspension. After 72hr, 20µL of MTT was added and kept in the CO_2 incubator for 2hr followed by addition of 100µL propanol. The plate was covered with aluminum foil to protect from light. Then the 27 well plates were kept in a rotary shaker for 10-20min. After 10-20 min, the 27 well plates were processed on an ELISA reader for absorption at 562nm.

2.1.6. Studies of molecular docking

Autodock vina 1.1.2 was used to study the interaction, binding mode between compounds **1f, 1g, fluorouracil** and the protein 4FM9 (Trott and Olson, 2010). The action of topoisomerase I and II determines the topological states of DNA (Wang et al. 2002). Replication, recombination, transcription, and DNA repair are all biological processes that rely on its functioning (Bertozzi et al. 2011, 2014; Marinello et al. 2013). Keeping this in mind, we chose topoisomerase II alpha bound to DNA (PDB ID: 4FM9) as our molecular docking target protein. In order to conduct cytotoxic screening, the structure of topoisomerase II alpha bound to DNA (PDB ID: 4FM9) was

downloaded from Protein Data Bank (http://www.rcsb.org). The 3D structures of compounds **1f**, **1g**, and **fluorouracil** were created with Chem3D Pro 12.0. AutoDock Tools 1.5.6 was used to create in put files. According to the search grid, the dimensions of the 4FM9 are size_x: 14, size_y: 16, and size_z: 16 resulting in a spacing of 1.0 Å. A score of 8 was assigned to exhaustiveness. The other parameters of the Vina docking were set to default. Based on Discovery studio 2019 results, the lowest binding affinity conceder as the highest score.

3. Results and discussion

3.1.9. Vibrational assignments

3.1.9.1. N-H vibrations

Three vibrations are generated by the N-H group (stretching, inplane bending, and out-of-plane bending). In the hydrogen-bonded species, the spectra of the vibrational N-H groups respond most strongly to the environment. In general, amine stretching vibrations are observed around 3300 cm^{-1}. The band at 3487.70 cm^{-1} [mode no: 86] with the strong FT-IR band at 3358.93 cm^{-1}, B3LYP is recognised to stretching vibrations N-H stretching.

3.1.9.2. C-H vibrations

The C-H stretching vibrations were obtained at 3100–3000 cm^{-1}. The strength of these vibrations is not affected by substituent nature and position, and they usually exhibit weaker bands than aliphatic stretching vibrations. The C-H stretching bands in ring C-H compounds cause most aromatic compounds to show approximately four peaks in the region 3080–3010 cm^{-1} on infrared spectra. The C-H bands depend on sp hybridization. The scaled vibrations, [mode no's: 85–80] computed by B3LYP/6-311G (d,p) method in the range 3199–3151 cm^{-1} show good contract with the recorded weak FT-IR band at 3176 cm^{-1}. In-plane C-H bending vibrations normally ensue in the range of 1300–1000 cm^{-1}, and it is very useful to characterize these vibrations. It is attributed to C-H in plane-bending vibrations that the FT-IR spectrum shows a strong peak at 1100.73 cm^{-1}. Based on theoretical computations, these values are in good agreement with B3LYP method at 1112.20 cm^{-1} [mode no: 49]. There was a mixture of vibrations C=C and C-C observed in these vibrational modes. Vibrations occurring out of plane of C-H are strongly coupled and range from 1000 to 600 cm^{-1}. The C-H modes with the highest wavenumbers have generally weaker intensities than modes with lower wavenumbers. In the FT-IR spectrum of the

title molecule compound 1a, the peak at 694.72 cm^{-1} confirms that the C-H bond is bent out-of-plane. Based on the theoretically scaled harmonic wavenumber for B3LYP, it is very close to the measured value at 650.73 cm^{-1} [mode no: 27].

3.1.9.4. C=O vibrations

Carbon and oxygen form a double bond by forming p_π–p_π bonds. In the case of oxygen and carbon, the electrons of their bond do not have the same electro negativities. A carbonyl group vibration normally occurs in the range 1780-1680 cm^{-1}. FT-IR measurements in the present study assign the -C=O stretching vibration to an experimental wavenumber at 1625.19 cm^{-1}, which matches B3LYP at 1618.93 cm^{-1}.

3.1.9.5. CH_3 vibrations

Compound **1a** should exhibit stretching and bending vibrations due to its attached CH_3 group, which expected to have asymmetry stretching vibrations occur between 3100 and 2905 cm^{-1}, and symmetric stretching vibrations, which occur between 3000 and 2860 cm^{-1}. CH_3 asymmetric stretching vibration is assigned at 3071.90 cm^{-1} [mode no: 79] by B3LYP method, for the methyl group at 3019.62 cm^{-1} [mode no: 77]. According to FT-IR experiments, it is well in agreement with the measurement at 3179 cm^{-1}. The B3LYP method has identified the in-plane bending vibrations (scissoring) of CH_3 group at 1467.88, 1458.44 cm^{-1} (mode no's: 63, 64), according to FT-IR experiments observed value at 1421.62 cm^{-1}.

3.1.9.6. Ring vibrations

Stretching vibrations of carbon–carbon occur between 1625 and 1430 cm^{-1}. In general, there are five bands in the region that have varied intensities, with six bands observed at 1625–1575, 1540–1470, 1465–1430, and 1380–1280 cm^{-1}. C=C stretching vibrations are responsible for the wavenumber at 1516.52 cm^{-1} in this study. The theoretical values computed by B3LYP at 1505.51, 1541.64 cm^{-1} [mode no's: 67, 70, 62, 60] are excellently correlated with experimental data. Observed IR spectra indicate characteristic bands between 1600 and 1400 cm^{-1} resulting from aromatic stretching vibrations. There was a strong and very strong FT-IR band observed at 1421.62 cm^{-1}. FT-IR spectra of compound 1a show excellent agreement with the calculated band 1419.33 cm^{-1} at B3LYP level [mode no: 62]. This FT-IR value at 468.77 cm^{-1} is in good

agreement with that of the measured wavelength with calculated at 425.40 cm^{-1} for C-C in-plane bending vibration by B3LYP/6-311G (d,p) method (mode no: 15).

3.1.12. HOMO–LUMO analysis

It is very important in quantum chemistry to know the lowest unoccupied molecular orbital (LUMO) and the highest occupied molecular orbital (HOMO). (See Supporting Info). By determining the frontier orbitals, we can determine the interactions between molecules and other species. HOMO is understood as being the electrons donors of outermost orbital containing electrons. LUMO, on the other hand, is understood as being the innermost orbital containing electrons that can be accepted. The HOMO and LUMO energies are calculated using the B3LYP/6-311G (d,p) method. The transition absorption is mainly characterized by the electron excitation from HOMO to LUMO, which corresponds to the transition from the ground to the first excited state. The bond C-C, C-O, and the NH_2 bond are the most occupied molecular orbitals in compound 1a, while the bond C-C is occupied most by the LUMO. The atomic composition of the frontier molecular orbital is shown in figure 14

3.1.18. Molecular docking

In order to study the docking behavior between compounds **1f, 1g,** and the control **fluorouracil** with protein 4FM9, the Autodock Vina program was utilized. (See Supporting Info for full details), In protein-ligand interactions, hydrogen bonds play a major role, and bond distance between the H-donor and H-acceptor atoms is less than 3.5 Å (Taha et al., 2015). Hydrogen bond distances between compounds **1f**, **1g**, and control fluorouracil in respective proteins were less than 3.5 Å, which indicates strong hydrogen bonding between the compounds. Compounded **1f** has a stronger binding affinity (-6.5 kcal/mol) than compound 1g (binding affinity -6.1 kcal/mol) and control fluorouracil.

Hydrogen bonding interactions were involved with a residue of the amino acid Asp683 (bond length: 2.39). In hydrophobic interactions, Leu592, Pro593 and Glu682 amino acid residues were involved. Molecular bonding occurs between **1g** and 4FM9 through two hydrogen bonds. Hydrogen bonds were formed between amino acid residues Leu592 (bond length: 2.11) and Glu702 (bond length: 3.01). It was found that the amino acids Gln544, Ile577, Ser591, Pro593 and Leu685, Tyr686, Lys701 and Leu705 interact hydrophobically. Fluorouracil was connected three hydrogen bonds with receptor 4FM9. A hydrogen bonding interaction was found between

amino acids Leu685 (bond length: 2.24), Tyr590 (bond length: 2.72), and Gln542 (bond length: 2.81). A hydrophobic interaction is associated with the amino acid Tyr686. As shown in, figure 16 (See Supporting Info), and 17 (See Supporting Info), these residues of the 4FM9 protein interact hydrophobically with compounds **1f, 1g**, and **fluorouracil** through hydrogen bonds and hydrophobic interactions. Compared to control **fluorouracil,** compound **1f** and compound **1g** had their best inhibitory properties in cytotoxic proteins.

3.1.19. Molecular Property Prediction and ADME

In the development of therapeutic agents, bioactive compounds play a major role (Newby et al., 2015) (See Supporting Info for full details). Based on this study, hydrogen-bonding capacity, low polar surface area, intestinal absorption, and reduced molecular flexibility were the most significant predictors (Azam et al., 2012). Lipinski's "Rule of 5" is not violated by the compounds **1f, 1g,** and **fluorouracil** (Table 7). The number of rotatable bonds in these molecules ensures that they do not exhibit high conformational flexibility and are oral bioavailable. Topological polar surface area (tPSA) has been correlated with the property of blood-brain barrier as well as molecular transport over membranes (Ertl et al., 2000). The compounds having tPSA value of < 140 $Å^2$ passes criteria. (%Abs = >50) indicates that the compounds were highly bioavailable. In oral administration (>50%), the bioavailability was acceptable. In addition, compound **1f** and compound **1g** demonstrate moderate water solubility (-logS value > 4), but the water solubility of fluorouracil (-logS value of –0.58) is excellent. Since **1f, 1g,** and **fluprpuracil** were not predicted as CYP2D6 inhibitors, liver dysfunction was not expected to occur. A P-glycoprotein (P-gp) is tested for drug metabolism brain diffusion, intestinal absorption, and their inhibition can have a dramatic impact on protective systems (Fromm, 2000). The effects of the drug are based on additional phospholipids formed in tissues, and that is associated with any toxic effects (Nonoyama and Fukuda, 2008). Neither **1f**, **1g**, nor **fluorouracil** caused phospholipidosis or P-gp in the tested compounds. In accordance with the ADME and toxicity results, **1f**, **1g**, and **fluorouracil** show reasonably good pharmacokinetic properties, and they are considered to be of drug-like properties, exceeding Lipinski's "Rule of 5" without violation.

References

Becke, A.D., 1993. Density-functional thermochemistry. III. The role of exact exchange, J. Chem. Phys. 98, 5648-5652. https://doi.org/10.1063/1.464913

Bertozzi, D., Iurlaro, R., Sordet, O., Marinello, J., Zaffaroni, N., Capranico, G., 2011. Characterization of novel antisense HIF-1α transcripts in human cancers. Cell Cycle. 10, 3189-3197. doi: 10.4161/cc.10.18.17183.

Bertozzi, D., Marinello, J., Manzo, S.G., Fornari, F., Gramantieri, L., Capranico, G., 2014. The natural inhibitor of DNA topoisomerase I, camptothecin, modulates HIF-1α activity by changing miR expression patterns in human cancer cells. Mol Cancer Ther. 13, 239-248. doi: 10.1158/1535-7163.MCT-13-0729.

Foresman, J.B., Keith, T.A., Wiberg, K.B., Snoonian, J., Frisch, M.J., 1996. Solvent effects. 5. Influence of cavity shape, truncation of electrostatics, and electron correlation on ab initio reaction field calculations. J. Phys. Chem. 100, 16098-16104. https://doi.org/10.1021/jp960488j

Frisch, M.J., Trucks, G.W., Schlegel, H.B., et al., 2010. Gaussian 09, Revision B.01, Gaussian, Inc., Wallingford CT.

Hariharan, P.C., Pople, J.A., 1973. The Influence of Polarization Functions on Molecular Orbital Hydrogenation Energies. Theor. Chim. Acta. 28, 213-222. https://doi.org/10.1007/BF00533485

Lee, C., Yang, W., Parr, R.G., 1988. Development of the Colle-Salvetti correlation-energy formula into a functional of the electron density. Phys. Rev. B. 37, 785-789. https://doi.org/10.1103/PhysRevB.37.785

Lipinski, C.A., Lombardo, F., Dominy, B.W., Feeney, P.J., 2001. Experimental and computational approaches to estimate solubility and permeability in drug discovery and development settings. Adv. Drug. Deliv. Rev. 46, 3-26. https://doi.org/10.1016/S0169-409X(96)00423-1

Marinello, J., Chillemi, G., Bueno, S., Manzo, S.G., Capranico, G., 2013. Antisense transcripts and R-loops caused by DNA topoisomerase I inhibition by camptothecin at

human active CpG island promoters. Cancer. Res. 73, (8 Supplement). doi:10.1158/1538-7445.AM2013-637

Montgomery, J.A., Frisch, M.J., Ochterski, J.W., Petersson, G.A., 1999. A complete basis set model chemistry. VI. Use of density functional geometries and frequencies. J. Chem. Phys. 110, 2822-2827. https://doi.org/10.1063/1.477924

Rohlfing, M., Leland, C., Allen, C., Ditchfield, R., 1984. Proton and carbon-13 chemical shifts: comparison between theory and experiment. Chem. Phys. 87, 9-15. https://doi.org/10.1016/0301-0104(84)85133-2

Stephens, P.J., Devlin, F.J., Chabalowski, C.F., Frisch, M.J., 1994. Ab initio calculation of vibrational absorption and circular dichroism spectra using density functional force fields. J. Phys. Chem. 98, 11623-11627. https://doi.org/10.1021/j100096a001

Surendra Kumar, R., Moydeen, M., Al-Deyab, S.S., Aseer, M., Idhayadhulla, A., 2017. Synthesis of new morpholine-connected pyrazolidine derivatives and their antimicrobial, antioxidant, and cytotoxic activities. Bioorg. Med. Chem. Let. 27, 66-71. https://doi.org/10.1016/j.bmcl.2016.11.032

Swiss ADME. Available online: http://www.swissadme.ch (accessed on 10 August 2021).

Tomasi, J., Mennuci, B., Cammi, R., 2005. Quantum mechanical continuum solvation models. Chem. Rev. 105, 2999-3094. https://doi.org/10.1021/cr9904009

Trott O., Olson, A.J., 2010. AutoDock Vina: Improving the speed and accuracy of docking with a new scoring function, efficient optimization, and multithreading. J. Comput. Chem. 31, 455-461. https://doi.org/10.1002/jcc.21334

Wang, S., Miller, W., Milton, J., Vicker, N., Stewart, A., Charlton, P., Denny, W.A., 2002. Structure–activity relationships for analogues of the phenazine-based dual topoisomerase I/II inhibitor XR11576. Bioorg. Med. Chem. Lett. 12, 415-418. doi: 10.1016/S0960-894X(01)00770-3.

Wolinski, K., Hinton, J.F., Pulay, P., 1990. Efficient implementation of the gauge-independent atomic orbital method for NMR chemical shift calculations. J. Am. Chem. Soc. 112, 8251- 8260. https://doi.org/10.1021/ja00179a005

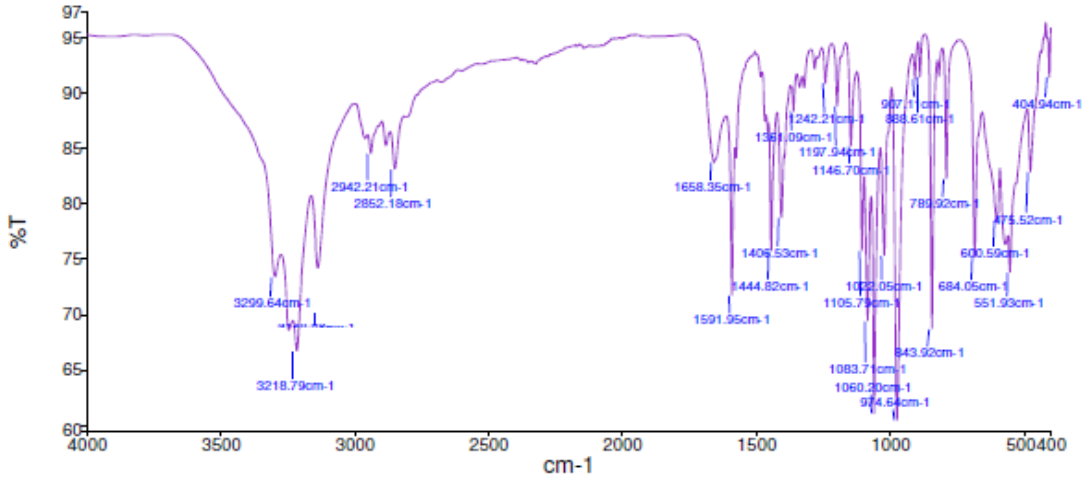

Figure 7, IR spectrum of **AEEA- Cu(II)-Nps**

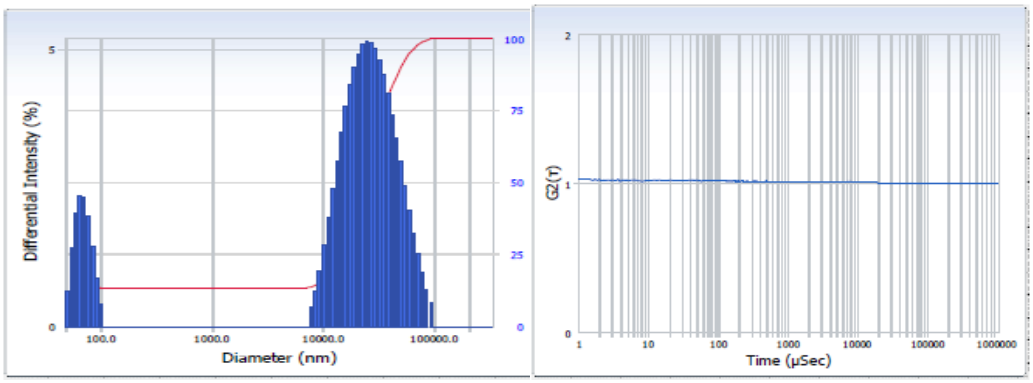

Distribution Results (Contin)

Peak	Diameter (nm)	Std. Dev.
1	70.7	12.8
2	32,009.1	17,943.6
3	0.0	0.0
4	0.0	0.0
5	0.0	0.0
Average	27,674.7	19,948.0
Residual :	1.446e-003	(O.K)

Cumulants Results

Diameter	(d)	: 6764.0	(nm)
Polydispersity Index	(P.I.)	: 2.014	
Diffusion Const.	(D)	: 1.180e-009	(cm²/sec)

Measurement Condition

Temperature	: 25.0	(°C)
Diluent Name	: Methanol	
Refractive Index	: 1.3312	
Viscosity	: 0.5470	(cP)
Scattering Intensity	: 32892	(cps)
Attenuator 1	: 100.0	(%)

Figure 8, Particle size distribution of **AEEA- Cu(II)-Nps**

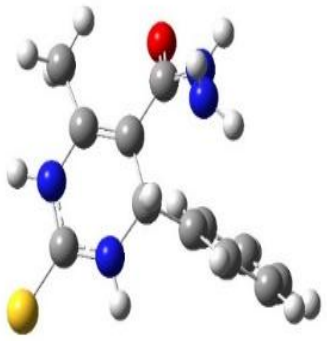

Figure 9. Possible conformer of compound 1a

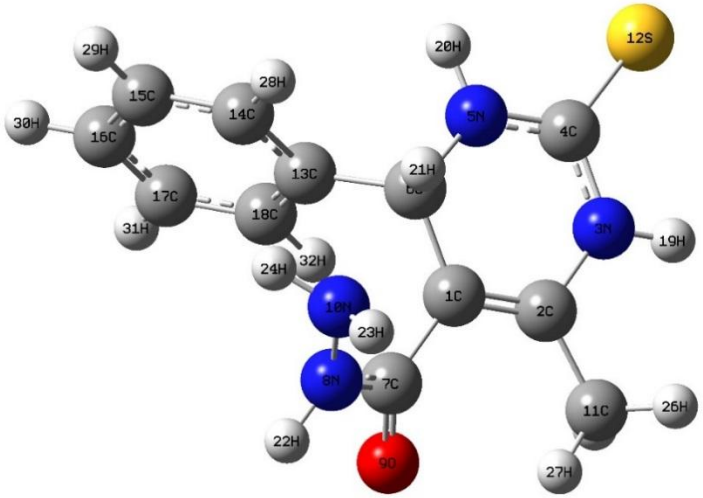

Figure 10. Optimized structure of compound 1a

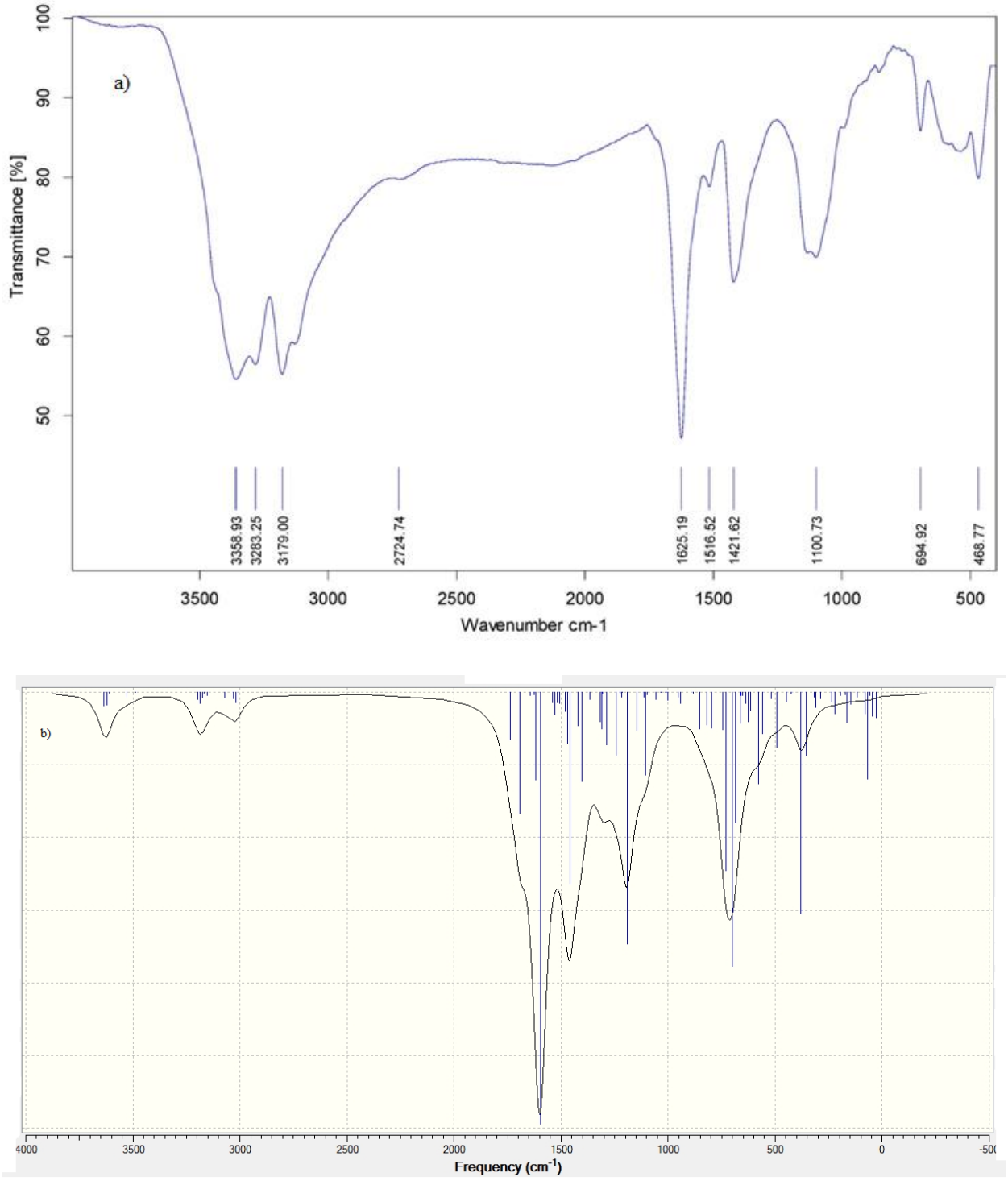

Figure 11, FT- IR spectra of (a) compound **1a**-experimental, (b) compound **1a** -theoretical.

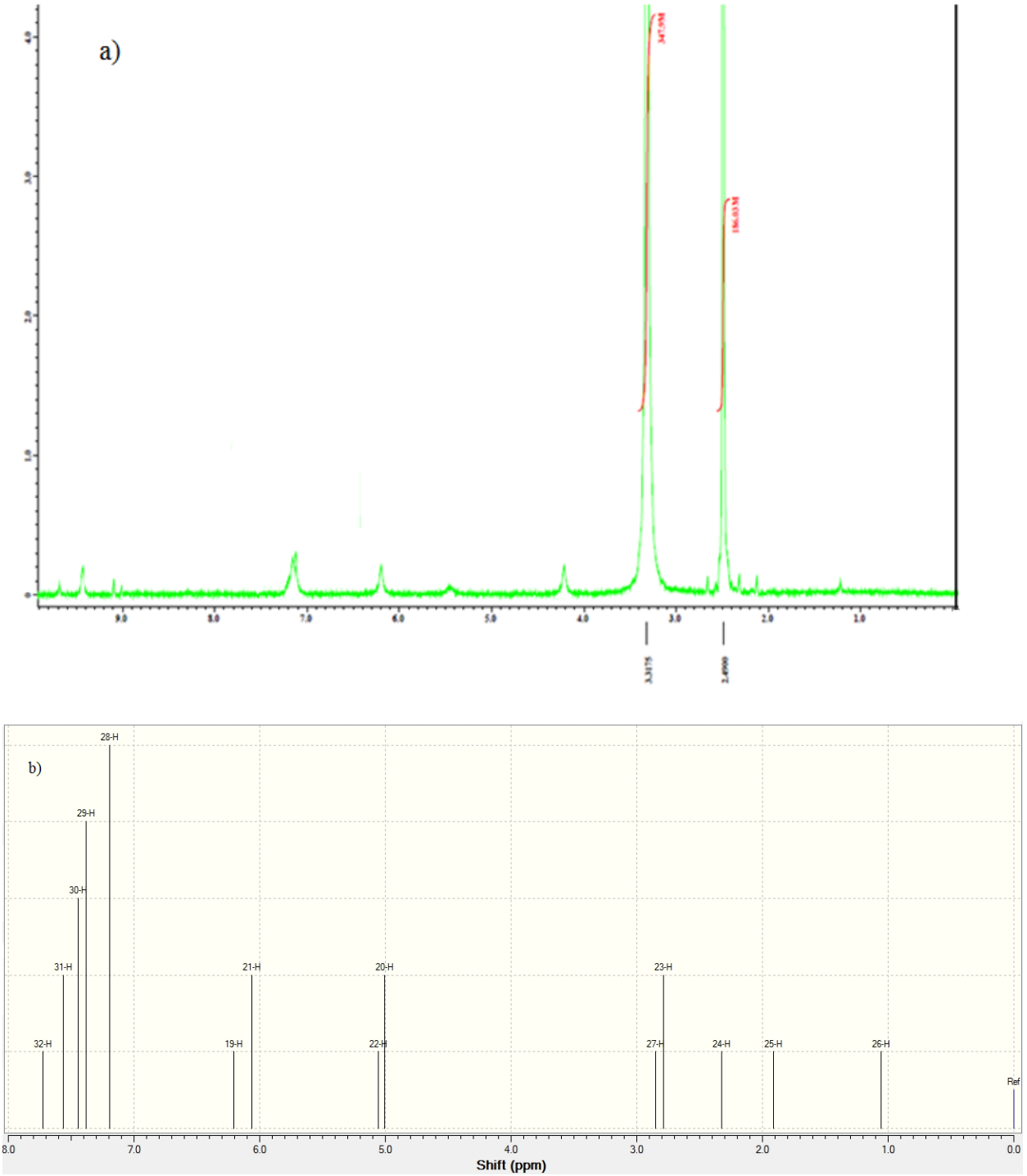

Figure 12, The observed (a) and calculated (b) ^{1}H NMR spectra of compound **1a**

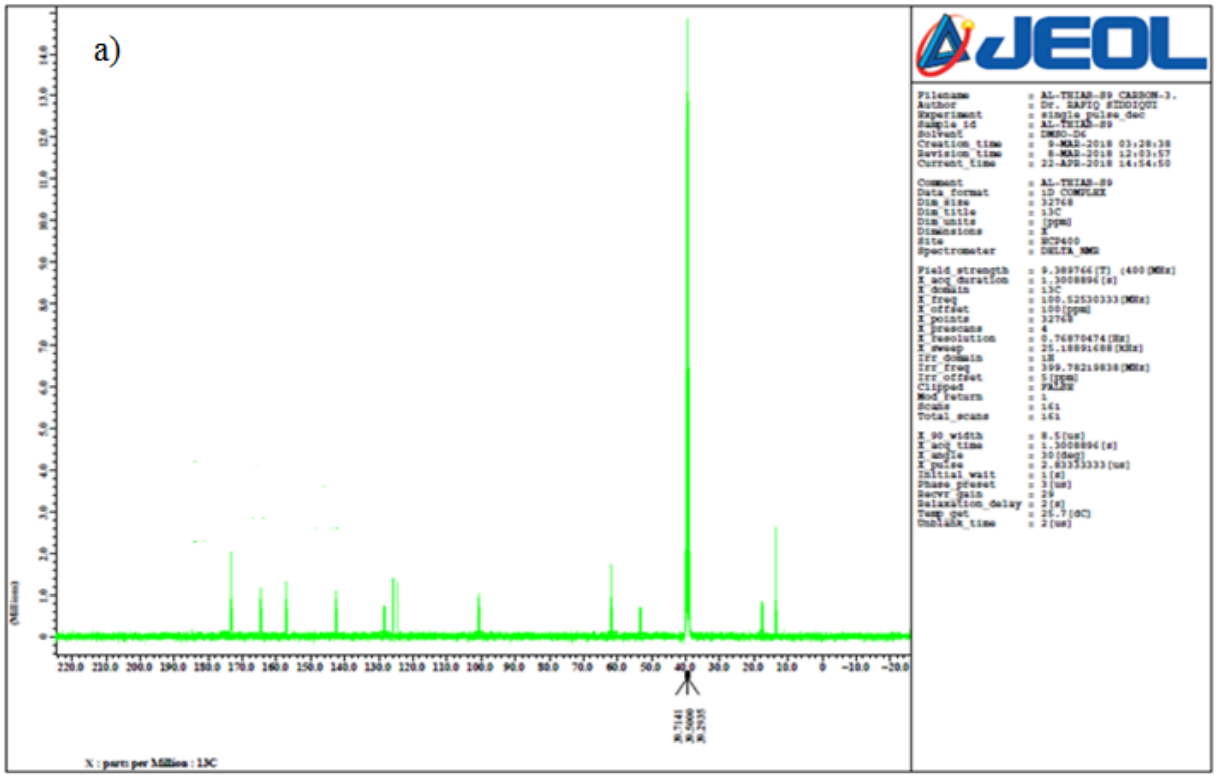

Figure 13, The observed (a) and calculated (b) ^{13}C NMR spectra of compound **1a**

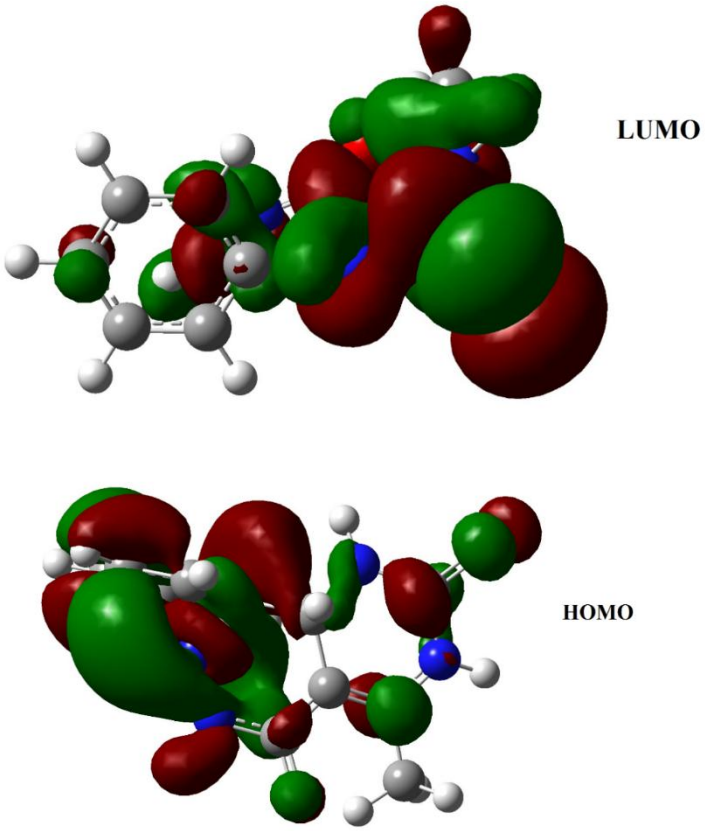

Figure 14, HOMO-LUMO plots of compound 1a.

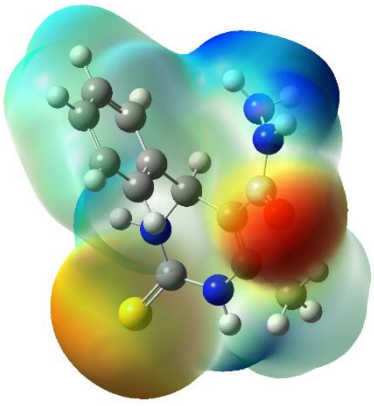

Figure 15, Molecular electrostatic potential map of compound 1a.

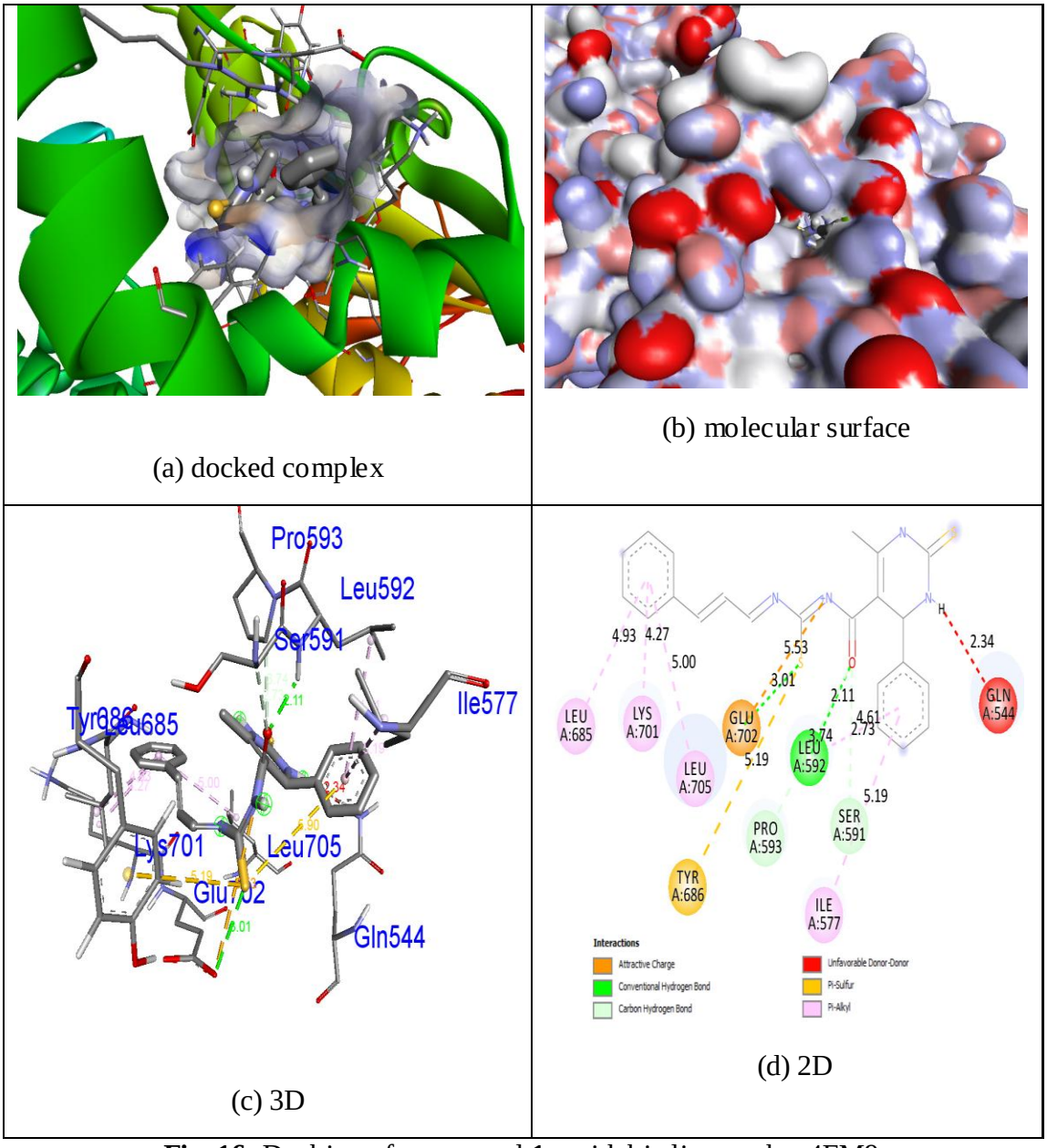

Fig. 16. Docking of compound **1g** with binding pocket 4FM9

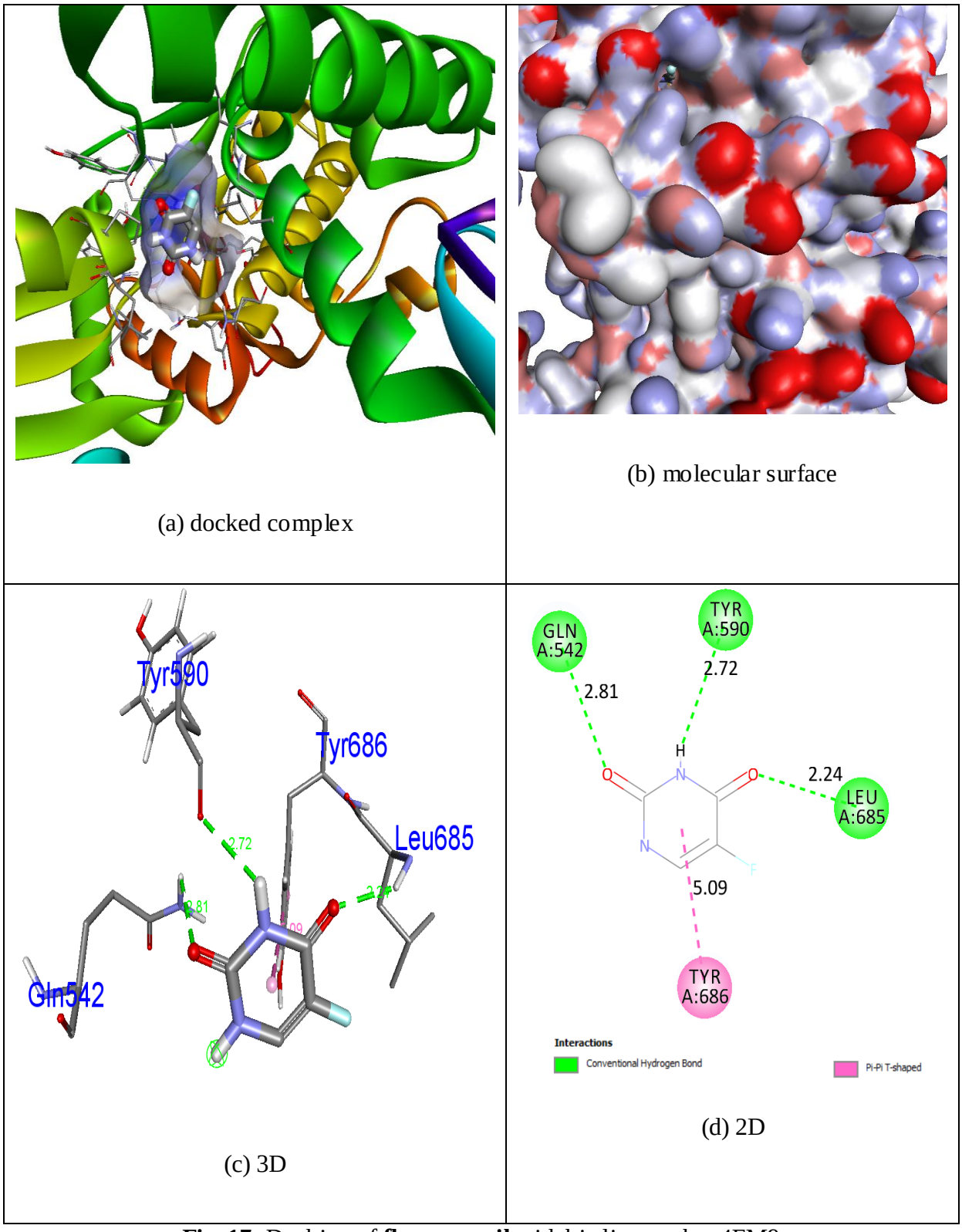

Fig. 17. Docking of **fluorouracil** with binding pocket 4FM9

Table 2 Parameter optimization for compound 1a

Bond lengths (Å)					
C1-C2	1.3585	N5-C6	1.4927	C13-C14	1.4016
C2-C11	1.5049	C6-H21	1.0912	C14-H28	1.0838
C2-N3	1.4014	C6-C13	1.5287	C14-C15	1.3985
N3-H19	1.0062	C1-C7	1.4821	C15-H29	1.0820
C11-H25	1.0927	C7-O9	1.2586	C15-C16	1.3965
C11-H26	1.0935	C7-N8	1.3788	C16-H30	1.0817
C11-H27	1.0825	N8-N10	1.4007	C16-C17	1.3987
N3-C4	1.3752	N8-H22	1.0126	C17-H31	1.0817
C4-S12	1.7260	N10-H23	1.0111	C17-C18	1.3965
C4-N5	1.3462	N10-H24	1.0106	C18-H32	1.0816
N5-H20	1.0074				
Bond angles (^{o})					
C1-C2-C6	31.8	C2-N3-C4	124.7	C13-C14-H28	119.4
C1-C2-C7	31.6	C4-N3-H19	115.5	C13-C18-H32	119.5
C1-C2-C11	127.2	N3-C4-S12	121.3	C13-C14-C15	120.6
C1-C2-N3	120.0	N3-C4-N5	114.9	C14-H28-C15	34.2
C1-C7-N8	119.8	C4-N5-S12	24.3	C14-C15-C16	119.9
C1-C7-O9	122.7	C4-N5-H20	115.9	C14-C15-H29	119.9
C7-N8-O10	124.8	C4-N5-C6	27.9	C15-C16-H29	25.7
C7-N8-O9	117.3	N5-H20-C6	38.4	C15-C16-H30	120.1
C7-N8-H22	114.2	N5-H20-H21	106.0	C15-C16-C17	119.7
N10-H23-H24	32.8	N5-H21-C6	42.2	C16-C17-H30	34.1
C2-C11-H25	110.1	C6-C13-C18	121.2	C16-C17-H31	120.0
C2-C11-H26	109.9	C6-C13-C14	119.6	C16-C17-C18	120.2
C2-C11-H27	112.1	C6-C13-H21	107.5	C17-C18-H31	119.7
C2-N3-H19	119.2	C13-C14-C18	30.5	C18-C13-H32	25.9
Dihedral angles (^{o})					
C1-C2-N3-C4	-11.7	S12-C4-N5-H20	2.0	C7-N8-N10-H24	121.5
C1-C2-C11-H25	106.3	S12-C4-N5-C6	-171.6	H32-C18-C13-C14	-179.9
C1-C2-C11-H26	55.5	C4-N5-C6-C13	-145.0	C18-C13-C14H28	-179.2
C1-C2-C11-H27	-12.5	H20-N5-C6-C13	41.3	C13-C14-H28-C15	179.5
C1-C2-C7-O9	150.1	H20-N5-H21-C6	116.3	C14-H28-C15-H29	179.8
C1-C2-N3-H19	136.9	N5-H21-C6-C4	26.4	C14-C15-C16-H30	-179.7
C2-N3-C11-H26	-138.2	C6-C13-C14-H28	-2.3	C15-C16-H30-C17	179.8
C11-C2-N3-H19	-2.8	C6-C13-C18-H32	3.1	H30-C16-C17-H31	179.9
C2-N3-C4-H19	-171.5	C1-C6-C13-C8	141.2	H31-C17-C18-H30	0.0
C2-N3-C4-S12	-176.8	C6-C1-H21-C13	35.9	H31-C18-C17-H32	0.2
N3-C4-H19-S12	0.7	O9-C7-N8-H22	175.9	C18-C17-H32-C13	0.3

Table 3 Calculated scaled wave numbers, IR bands and assignments for compound **1a**

B3LYP/6311G (d,p) ν (cm^{-1})	IR ν (cm^{-1})	Assignments
3635.84	-	symNH_2
3619.24	-	asyNH_2
3611.47	-	asyNH
3529.15	3283.25	NH_2
3487.70	3358.93	symNH
3199.16	-	CH Str
3187.04	-	CH Str
3176.86	3179.00	Ar CH Str
3176.81	-	CH Str
3167.01	-	CH Str
3151.06	-	CH Str
3071.90	3179	symCH_3
3019.62	-	asymCH_3
1618.93	1625.19	C=O
1541.64	-	Ar Ring
1505.51	1516.52	C=C str
1419.33	1421.62	Ar Ring str
1364.81	-	In plane CH bending
1225.43	-	In plane CH bending
1211.78	-	C-H In plane bending
1112.20	1100.73	C-H In plane bending
1055.61	-	C-H In plane bending
1033.44	-	C-H In plane bending
1030.55	-	C-H In plane bending
1007.05	-	C-H In plane bending
953.37	-	C-H In plane bending
425.40	468.77	C-C In plane bending
318.54	-	C-C out of plane bending

Table 4 A theoretical and experimental NMR spectrum of compound **1a** (in ppm)

Atoms	Exp.	B3LYP/6-311G (d,p)	Atoms	Exp.	B3LYP/6-311G (d,p)
C4	174.2	185.9	H32	7.20	7.72
C7	165.0	179.4	H31	-	7.56
C13	158.0	150.1	H30	-	7.44
C2	143.0	147.9	H29	6.20	7.38
C18	128.3	135.6	H28	5.50	7.19
C17	-	134.8	H19	9.20	6.20
C16	-	133.2	H21	4.20	6.06
C15	127.1	132.3	H22,20	9.40	5.03
C14	126.5	130.9	H27	-	2.85
C1	100.0	108.4	H23	-	2.78
C6	54.0	63.3	H24	2.10	2.32
C11	18.0	14.0	H25	-	1.91
			H26	1.20	1.05